Radiation Loss of Y-Junctions in Rib Waveguide

Lucia Cascio, Tullio Rozzi, *Fellow, IEEE*, and Leonardo Zappelli

***Abstract*—In this paper we analyze the effects of radiation in Y-junctions in rib waveguide by combining the effective dielectric constant method and the concept of local modes of a five-layer slab guide. The evaluation of the fields of the junction is performed together with the analysis of the radiation effects at the end of the transition; various kinds of junctions are examined and discussed, in both LSE and LSM polarizations.**

I. Introduction

THE Y-JUNCTION in dielectric waveguide is a fundamental tool in integrated optics and in the high millimetric region while offering promise for millimetric circuits with a view to realizing power dividers, directional couplers and spatial diplexers. The bidimensional Y-junction has been studied in several ways in the literature, from the late 1970's to date [1]–[6]. These studies evaluate the coupling between guided modes of the slab structure constituting the Y-junction [1]–[3], [5], [6], but only in [4] radiation modes are considered, to some extent, by discretization in terms of known functions; radiated power is then approximately evaluated.

Three dimensional Y-junctions, instead, are studied by means of numerical methods, such as the beam propagation method or the finite element method [7]–[9].

An important feature of the Y-junction, that seems to have been neglected so far, is the presence of a radiation lobe emitted at the vertex of the Y and propagating between its two arms, corresponding to a resistively loaded fourth arm of the junction; this effect alters the spatial diplexing characteristics and could be of relevance in densely packed switching matrices.

In this paper we consider the Y-junction under both LSE and LSM polarizations, using the EDC method in the vertical (y) direction, then applying local modes analysis [10], [11] to the resulting five-layer structure in the transverse (x) direction and taking into account radiation modes in the transition. We investigate propagation in the two arms of the Y-junction and radiation occurring between them. It is to be noted that, although the local modes approach is electromagnetically rigorous, as a consequence of applying the EDC method in the y-direction, we do not account for radiation in the y-z plane but in the x-z plane only. The exact computation of radiation effects in the three-dimensional space can be carried out by introducing the exact continuous modes of the rib waveguide, as reported in [12]. Nevertheless, in this paper, we resort to the EDC method to produce a relatively simple and efficient code still capable of modeling accurately radiation at the vertex of the Y.

Manuscript received December 16, 1993; revised April 24, 1995. This work was supported by the EEC Commission under the SCIENCE scheme, Contract SCI-CT91-0634.

The authors are with the Dipartimento di Elettronica ed Automatica, Università degli Studi di Ancona, Via Brecce Bianche, 60131 Ancona, Italy.

IEEE Log Number 9412695.

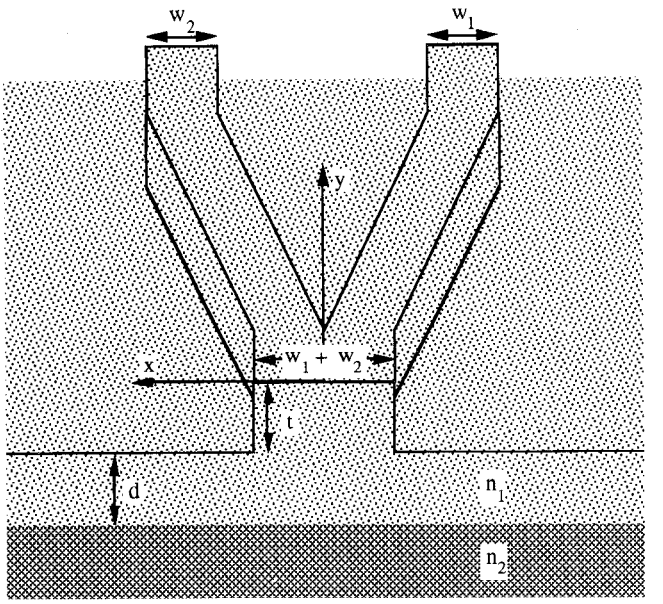

Fig. 1. The Y-junction in rib waveguide. The refraction indices are n_1 and n_2, with $n_1 > n_2$.

II. Theory

The Y-junction in rib waveguide is shown in Fig. 1. The first step of the analysis consists in applying the EDC method in the y-direction (LSE polarization), obtaining a five-layer structure extending in the x-direction, as shown in Fig. 2. In the x-z plane, the main polarization is now TM.

Fields are not easily representable in the transition region. In this paper, we expand the fields in terms of local modes, i.e., the orthonormal modes of the straight five-layer structure locally coincident with the cross section. These comprise a guided and a continuous contribution [13]. The rigorous expression of the $H_y(x,z)$ component in the five-layer structure expressed in terms of the local modes is [10]

$$H_y(x,z) = \sum_{k=-N}^{N} C_k(z)\Phi_k[x,(z)] + \sum_{\mu=\pm}\int_0^{\infty} C_\mu(\rho,z)\Phi_\mu[\rho,x,(z)]\,d\rho \quad (1)$$

where $\Phi_k[x,(z)]$ and $\Phi_\mu[\rho,x,(z)]$ represent the magnetic component of the guided local modes and continuous even and odd modes respectively, as reported in [13], and $C_k(z)$ and $C_\mu(\rho,z)$ are unknown coefficients, ρ is the independent

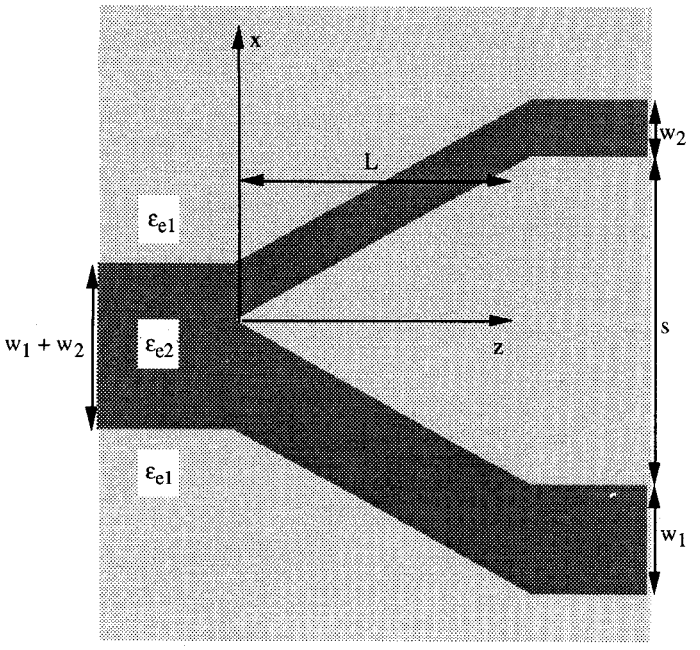

Fig. 2. The Y-junction after the application of the EDC method. The EDC method reduces the structure to a five-layer one varying along the z-direction. The effective dielectric constants are ε_{e1} and ε_{e2} with $\varepsilon_{e2} > \varepsilon_{e1}$.

variable of the continuous modes, N is the number of the guided local modes. In (1) the minus stands for backward propagating modes, either guided and continuous. The contribution of the continuum comprizes those of the even and odd parities, even though not explicitly indicated. Local modes are direct functions of x only, but there is a weak dependence on z too, due to the variation of geometry along the z-axis.

The axial (z) derivative of $H_y(x,z)$, that is proportional to the E_x-component, is expressed as

$$\frac{\partial H_y(x,z)}{\partial z} = -j\sum_{k=-N}^{N}\beta_k(z)C_k(z)\Phi_k[x,(z)] - j\sum_{\mu=\pm}\int_0^\infty \beta_\mu(\rho)C_\mu(\rho,z)\Phi_\mu[\rho,x,(z)]\,d\rho \quad (2)$$

where $\beta_\mu^2(\rho) = k_0^2\varepsilon_{e1} - \rho^2, k_0 = 2\pi/\lambda, \varepsilon_{e1}$ and ε_{e2} being the effective dielectric constants as shown in Fig. 2.

The solution of the propagating problem represented by (1) and (2) consists in determining the unknown coefficients $C_k(z)$ and $C_\mu(\rho,z)$.

Local modes are solutions of the following wave equation:

$$\varepsilon_e\frac{\partial}{\partial x}\left[\frac{1}{\varepsilon_e(x)}\frac{\partial\Phi(x)}{\partial x}\right] + [k_0^2\varepsilon_e(x) - \beta^2]\Phi(x) = 0 \quad (3)$$

with $\Phi(x) = \Phi_k(x)$ and $\beta = \beta_k$ for guided modes or $\Phi(x) = \Phi_\mu(\rho,x)$ and $\beta = \beta_\mu(\rho)$ for continuous modes, whereas, the actual fields in the Y-junction satisfy the following wave equation:

$$\varepsilon_e(x,z)\frac{\partial}{\partial x}\left[\frac{1}{\varepsilon_e(x,z)}\frac{\partial H_y(x,z)}{\partial x}\right] + \varepsilon_e(x,z)\frac{\partial}{\partial z}\left[\frac{1}{\varepsilon_e(x,z)}\frac{\partial H_y(x,z)}{\partial z}\right] + k_0^2\varepsilon_e(x,z)H_y(x,z) = 0. \quad (4)$$

Combining (1)–(4) by some manipulations, as reported in Appendix A, we obtain a system of coupled integro-differential equations for the amplitudes of the coupled local modes, namely

$$C_n'(z) + j\beta_n(z)C_n(z) = \sum_{k=-N}^{N}A_{nk}C_k(z) + \sum_{\mu=\pm}\int_0^\infty A_{n\mu}(\rho,z)C_\mu(\rho,z)\,d\rho, \quad n = -N\cdots N \quad (5)$$

$$C_\mu'(\rho,z) + j\beta_\mu(\rho)C_\mu(\rho,z) = \sum_{k=-N}^{N}D_{\mu k}(\rho,z)C_k(z) + \sum_{\nu=\pm}\int_0^\infty D_{\mu\nu}(\rho,\tilde\rho,z)C_\nu(\tilde\rho,z)\,d\tilde\rho, \quad \mu = \pm \quad (6)$$

where the apex stands for derivation with respect to z and $A_{nk}(z), A_{n\mu}(\rho,z), D_{\mu k}(\rho,z)$, and $D_{\mu\nu}(\rho,\tilde\rho,z)$ are the cross coupling coefficients between guided and continuous modes, as reported in the Appendix A. In the following we neglect cross-coupling between continuous modes, that is negligible indeed, i.e., we set $D_{\mu\nu}(\rho,\tilde\rho,z) \approx 0$.

A more effective form of (5) and (6) can be obtained by factoring out the rapid phase variation with z, i.e., by setting

$$C_n(z) = \frac{H_n(z)}{\sqrt{|\beta_n(z)|}}e^{-j\gamma_n(z)}$$
$$\gamma_n(z) = \int_0^z \beta_n(t)\,dt$$
$$C_\mu(\rho,z) = \frac{H_\mu(\rho,z)}{|\beta_\mu(\rho)|}e^{-j\beta_\mu(\rho)z}$$

so that (5) and (6) become

$$H_n'(z) = \sum_{k=-N}^{N}A_{nk}(z)(1-\delta_{nk})H_k(z)\sqrt{\left|\frac{\beta_n(z)}{\beta_k(z)}\right|}\cdot e^{-j[\gamma_k(z)-\gamma_n(z)]} + \sum_{\mu=\pm}\int_0^\infty A_{n\mu}(\rho,z)H_\mu(\rho,z)\cdot\frac{\sqrt{|\beta_n(z)|}}{|\beta_\mu(\rho)|}e^{-j[\beta_\mu(\rho)z-\gamma_n(z)]}\,d\rho, \quad n = -N\cdots N \quad (7)$$

$$H_\mu'(\rho,z) = \sum_{k=-N}^{N}D_{\mu k}(\rho,z)H_k(z)\frac{|\beta_\mu(\rho)|}{\sqrt{|\beta_k(z)|}}\cdot e^{-j[\gamma_k-\beta_\mu(\rho)z]} \quad \mu = \pm. \quad (8)$$

Due to the presence of the continuum integral, the analytical solution of (7) and (8) is not simple: straightforward numerical integration, e.g., by the Runge–Kutta method, is not applicable because of the fact that ρ ranges from 0 to infinity so that an infinite number of unknowns is produced. To simplify the analysis, we now suppose that backward propagating modes,

either guided or continuous, are not excited in the transition, a well-founded assumption if the transition is smooth at its beginning. In this hypothesis, (7) and (8) become

$$H_n'(z) = \sum_{k=1}^{N} A_{nk}(z)(1-\delta_{nk})H_k(z)\sqrt{\frac{\beta_n(z)}{\beta_k(z)}} \cdot e^{-j[\gamma_k(z)-\gamma_n(z)]} + \sum_{\mu=e,o}\int_0^{\infty} A_{n\mu}(\rho,z) \cdot H_\mu(\rho,z)\frac{\sqrt{\beta_n(z)}}{\beta(\rho)}e^{-j[\beta(\rho)z-\gamma_n(z)]}\,d\rho \qquad n = 1\cdots N \tag{7a}$$

$$H_\mu'(\rho,z) = \sum_{k=1}^{N} D_{\mu k}(\rho,z)H_k(z)\frac{\beta(\rho)}{\sqrt{\beta_k(z)}} \cdot e^{-j[\gamma_k(z)-\beta(\rho)z]}, \qquad \mu = e,o \tag{8a}$$

where now the even and odd parity of the continuous modes is made explicit. In (7a) and (8a) we have considered that $\beta_e(\rho) = \beta_o(\rho) = \beta(\rho)$.

We solve (7a) and (8a) by the following numerical procedure: We divide the whole domain of integration, corresponding to the length L of the transition, in M sub-intervals, where the unknown coefficients of the guided modes are expanded as second degree polynomials, to ensure continuity of $H_n(z)$ and $H_n'(z)$ at each boundary between sub-intervals. Details are provided in Appendix B and results will be discussed in the following.

Finally, we considered the LSM polarization. In this case the EDC approach yields a five-layer structure under TE polarization in the x-direction, whose complete spectrum is reported in [13]. The corresponding system of equations representing propagation in the Y-junction is the same as (7a) and (8a), but with different coupling coefficients; the latter are reported at the end of Appendix A.

A. Coupling Between Modes: Some Considerations

The extent of the z-dependence of the coupling coefficients is directly related to the shape of the transition and to the form of the rib waveguides constituting the Y-junction.

Some interesting effects occur in case of a Y-junction in rib waveguide with identical arm widths $w_1 = w_2$ and symmetric with respect to the z-axis. In fact, the five-layer structure obtained by application of the EDC method in the y-direction is perfectly symmetrical, as shown in Fig. 3; in the figure, $f_1(z), f_2(z), f_3(z)$ and $f_4(z)$ represent the laws of variation of the transition along the z-direction.Thus, analyzing coupling between modes, with different parity, either guided and continuous, noting that

$$f_1'(z) = f_4'(z) \quad f_2'(z) = f_3'(z)$$

and that in (A.I.7) $T_{1nk} = -T_{4nk}, T_{2nk} = -T_{3nk}$, we obtain $A_{nk}(z) = 0$.

The same holds for the other coupling coefficients. Therefore, coupling between modes with different parity is not allowed. In the symmetric Y-junction coupling occurs between modes with the same parity only.

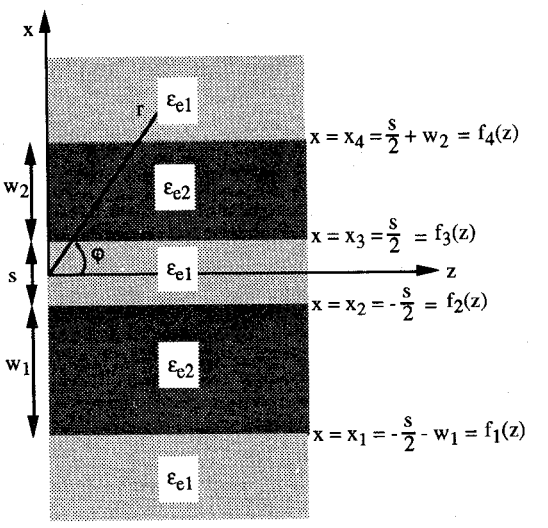

Fig. 3. The characteristics of the five-layer structure and the polar coordinate system used to evaluate the radiation pattern.

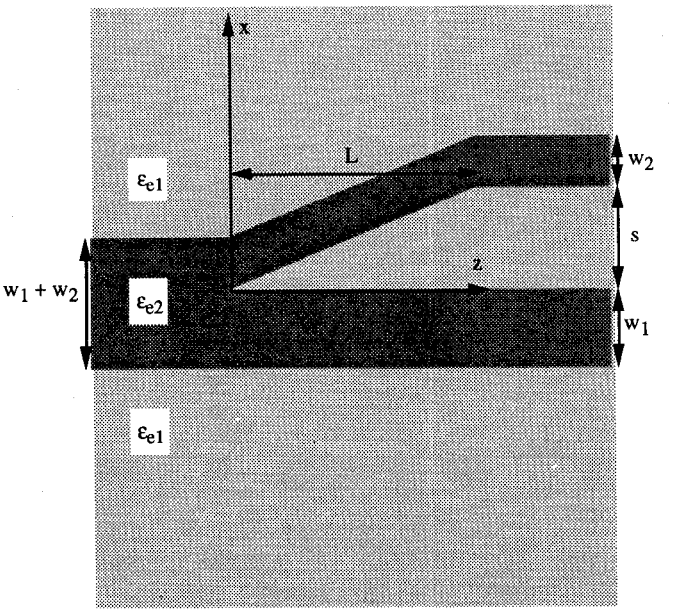

Fig. 4. The Y-junction with one arm only varying along the z-direction.

If the Y-junction has unequal arm widths, coupling between fundamental and first higher order mode and continuous modes is present even when the fundamental mode only is excited in the incoming rib waveguide; the same effects hold when just one arm of the Y-junction varies along z as shown in Fig. 4; in both cases, radiation occurs and it depends on the shape of the transition.

It is interesting to note that even when the arms of the junction are very far apart there is coupling between modes, either guided and continuous, that propagate on the same arm. This coupling is important in as much as the field that truly propagates is that in the ξ_1 (ξ_2) directions, relative to a three-layer guide with core-width $w_1\cos\theta(w_2\cos\theta)$, as shown in Fig. 5. When the two arms are very far apart, local modes of the five-layer guide reduce to the modes of the three layer guide with core width w_1 (w_2): therefore, to ensure the

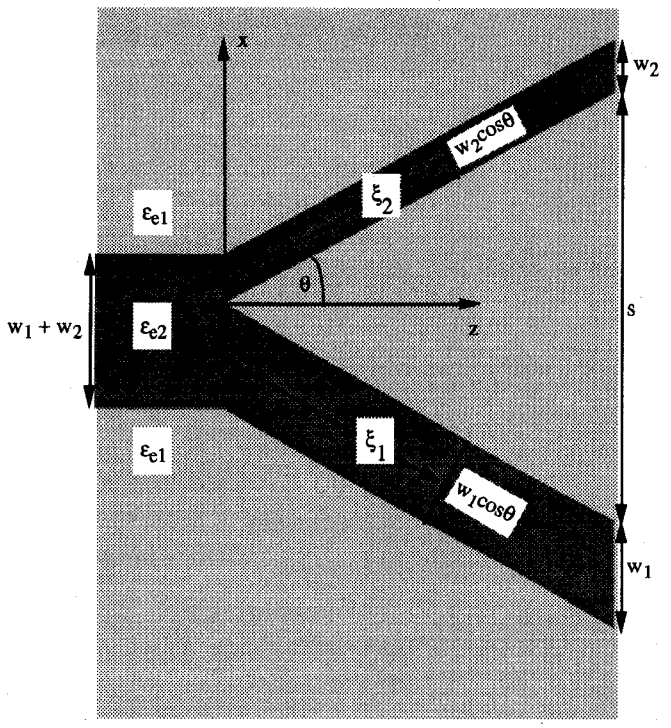

Fig. 5. The actual propagation directions of the fields in the two arms of the Y-junction.

presence of a real field propagating in the ξ_1 (ξ_2) directions, coupling between local modes can not vanish.

B. Radiation Pattern

Due to the excitation of continuous modes, radiation occurs at the Y-junction and we will examine its pattern by means of the saddle point method.

Starting from one end of the transition, the expression of the magnetic field in the uniform region is

$$H_y(x,z) = \sum_{\mu=e,o} \int_0^\infty \frac{H_\mu(\rho,L)}{\beta(\rho)} \Phi_\mu[\rho,x,(L)] e^{-j\beta(\rho)z}\, d\rho$$

where the expressions for $\Phi_\mu[\rho,x,(L)]$ are reported in [13]. Referring to Fig. 3, we introduce a polar co-ordinate system r,φ. Using the saddle point method, the expression of the radiated power for $r \to \infty$ is

$$P(\varphi) = \frac{1}{2} E_\varphi(r,\varphi) H_y^*(r,\varphi) r = \frac{Z_0}{2k_0\varepsilon_{e1}} \cdot \left| \sum_{\mu=e,o} \frac{H_\mu(\rho,L) e^{j\phi_{k\mu}(\rho)}}{\sqrt{\dfrac{1}{\varepsilon_{e1}} + \dfrac{v_{i\mu}^2(\rho)+u_{i\mu}^2(\rho)}{\varepsilon_{e1}[v_{k\mu}^2(\rho)+u_{k\mu}^2(\rho)]}}} \right|^2_{\rho=k_0 n_{e1}\sin\varphi} \tag{9}$$

where Z_0 is the free space impedance and

$$\phi_{i\mu}(\rho) = \arctan\left[\frac{u_{i\mu}(\rho)}{v_{i\mu}(\rho)}\right]$$

and $i=5, k=1$ for $-(\pi/2) \le \varphi \le -\arcsin(w_1+(s/2)/r)$ and $i=1, k=5$ for $\arcsin(w_2+(s/2)/r) \le \varphi \le \pi/2$.

Moreover, $\sigma = \sqrt{\rho^2 + k_0^2(\varepsilon_{e2}-\varepsilon_{e1})}$ and

$$\begin{aligned}
v_{1e}(\rho) &= \alpha_e \cos(\rho w_1) + \frac{\varepsilon_{e2}\rho}{\varepsilon_{e1}\sigma}\gamma_e \sin(\rho w_1)\\
u_{1e}(\rho) &= \frac{\varepsilon_{e1}\sigma}{\varepsilon_{e2}\rho}\alpha_e \sin(\rho w_1) - \gamma_e \cos(\rho w_1)\\
v_{5e}(\rho) &= \delta_e \cos(\sigma w_2) - \frac{\varepsilon_{e2}\rho}{\varepsilon_{e1}\sigma}\eta_e \sin(\sigma w_2)\\
u_{5e}(\rho) &= -\frac{\varepsilon_{e1}\sigma}{\varepsilon_{e2}\rho}\delta_e \sin(\sigma w_2) - \eta_e \cos(\sigma w_2)\\
\alpha_e &= \cos\left(\rho\frac{s}{2}\right) + \sin\left(\rho\frac{s}{2}\right)\tan\,\phi_e\\
\gamma_e &= -\sin\left(\rho\frac{s}{2}\right) + \cos\left(\rho\frac{s}{2}\right)\tan\,\phi_e\\
\delta_e &= \cos\left(\rho\frac{s}{2}\right) - \sin\left(\rho\frac{s}{2}\right)\tan\,\phi_e\\
\eta_e &= \sin\left(\rho\frac{s}{2}\right) + \cos\left(\rho\frac{s}{2}\right)\tan\,\phi_e\\
v_{1o}(\rho) &= \gamma_o \cos(\rho w_1) - \frac{\varepsilon_{e2}\rho}{\varepsilon_{e1}\sigma}\alpha_o \sin(\rho w_1)\\
u_{1o}(\rho) &= \frac{\varepsilon_{e1}\sigma}{\varepsilon_{e2}\rho}\gamma_o \sin(\rho w_1) + \alpha_o \cos(\rho w_1)\\
v_{5o}(\rho) &= \eta_o \cos(\sigma w_2) + \frac{\varepsilon_{e2}\rho}{\varepsilon_{e1}\sigma}\delta_o \sin(\sigma w_2)\\
u_{5o}(\rho) &= -\frac{\varepsilon_{e1}\sigma}{\varepsilon_{e2}\rho}\eta_o \sin(\sigma w_2) + \delta_o \cos(\sigma w_2)\\
\alpha_o &= \cos\left(\rho\frac{s}{2}\right) + \sin\left(\rho\frac{s}{2}\right)\tan\,\phi_o\\
\gamma_o &= -\sin\left(\rho\frac{s}{2}\right) + \cos\left(\rho\frac{s}{2}\right)\tan\,\phi_o\\
\delta_o &= \cos\left(\rho\frac{s}{2}\right) - \sin\left(\rho\frac{s}{2}\right)\tan\,\phi_o\\
\eta_o &= \sin\left(\rho\frac{s}{2}\right) + \cos\left(\rho\frac{s}{2}\right)\tan\,\phi_o.
\end{aligned}$$

In the previous expressions, ϕ_e and ϕ_o are reported in [13]. For $r \to \infty$, the range of (9) becomes $-(\pi/2) \le \varphi \le \pi/2$.

III. Results

To make a comparison with the literature, we tested our approach against two structures previously investigated.

First, we evaluated the power exchange between guided modes, neglecting the continuous contribution, occurring in a five-layer TE structure with a linear transition, as reported in [2], where guided modes only are taken into account. The linear transition has a branching angle θ and, referring to Fig. 6(a), the other parameters are $w_1 = w_2 = 0.95\lambda, n_1 = 1.474, n_2 = n_4 = 1.560, n_3 = n_5 = 1.473, \lambda = 1.15\ \mu$m. The power transferred from the fundamental TE_0 mode to the TE_1 mode versus the branching angle is compared in Fig. 6(b), against the data of [2]: continuous line refers to our approach, whereas dots refer to [2]. The agreement seems very good.

The second test we performed was the analysis of the coupling between the guided mode and the continuum occurring in a simple structure, namely a slab waveguide under TE polarization with sinusoidal varying walls.

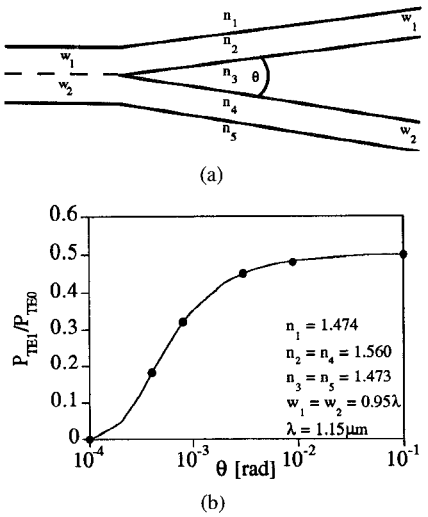

Fig. 6. (a) Geometry of the linear junction reported in [2]; (b) behavior of the transferred power from the fundamental TE_0 mode to the TE_1 mode versus the branching angle θ of the linear junction as reported in [2]. The continuous line refers to our approach whereas dots refer to [2].

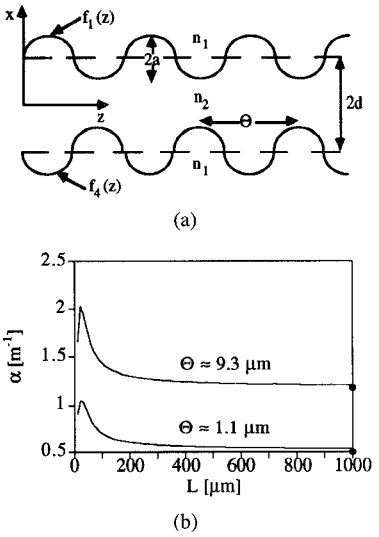

Fig. 7. (a) Geometry (not in scale) of the slab with sinusoidal varying walls as reported in [14]; (b) comparison between the power loss coefficient α ($P = P_0 e^{-2\alpha L}$) reported in [14] (dots) and those obtained by the present approach (continuous lines) for different values of the mechanical period $\Theta = 2\pi/\theta$.

Referring to Fig. 7(a) (not in scale), we have set $d = 2.39\ \mu\text{m}, n_1 = 1, n_2 = 1.01, \lambda = 1\ \mu\text{m}$, and $f_1(z) = -f_4(z) = d + a\sin(\theta z), a = 5.46 \cdot 10^{-2}\ \mu\text{m}$, as reported in [14]. An approximate semianalytical solution for the power loss exists [14] if the structure is considered very long [(9.3)–(19) of [14]]. The pitch θ of the perturbation that ensures coupling between the forward guided mode and the forward even radiation modes lies in the interval $0 \le \theta \le \beta_0 + k_0 n_1$, where β_0 is the propagation constant of the guided mode. We compared the approximate power loss coefficient α of the guided mode ($P = P_0 e^{-2\alpha L}$) reported in [14] and the results obtained by means of our approach varying the length L of the perturbation region.

Results are reported in Fig. 7(b), for some values of the mechanical period $\Theta = 2\pi/\theta$: dots are the theoretical results by [14] whereas the continuous lines refer to our approach. As the length of the perturbation region becomes longer, the curves tend to the dots.

Having checked the accuracy of the approach for these known cases, we studied the Y-junction, being the object of our work.

We examined first the linear transition shown in Fig. 1, in conjunction with a symmetrical Y-junction rib waveguide under LSE polarization, with the following parameters $n_1 = 3.44, n_2 = 3.40, t = 0.4\ \mu\text{m}, d = 0.6\ \mu\text{m}, \lambda = 1.15\ \mu\text{m}, w_1 = w_2 = 1.5\ \mu\text{m}, L = 60\ \mu\text{m}$ and final separation $s = 2\ \mu\text{m}$. The application of the EDC method in the y-direction yields a five TM layer with $n_{e1} = 3.40239, n_{e2} = 3.41715$.

We suppose that only one guided mode is excited with 1 W/m power (for unit length in the y direction), the even (fundamental) mode or the odd one. Due to the symmetry of the transition, coupling occurs between guided and continuous modes of the same parity only. Comparison between power of the guided mode and power of the continuous modes is reported in Fig. 8(a) for the even modes and in Fig. 8(b) for the odd modes; we note that the first case shows larger coupling between guided and continuous modes than the second does. This is due to the fact that odd modes have a vanishing $H_y(x,z)$-component on the plane of symmetry: consequently, the discontinuity has a minor effect and less power is transferred to the continuous modes than in the even case, where $H_y(x,z)$ shows a maximum on the plane of symmetry. If the final separation is doubled while keeping the same length L, coupling between modes increases, as shown in Fig. 8(c) and (d).

We also analyzed a symmetrical transition with a raised cosine profile ($s = 2\ \mu\text{m}$), characterized by

$$f_3(z) = -f_2(z) = \frac{s}{4}\left[1 + \sin\left(\pi \frac{z - \frac{L}{2}}{L}\right)\right]$$

$$f_4(z) = -f_1(z) = f_3(z) + w_2.$$

Coupling is lower than in the previous case at the extremities of the transition, but, it is stronger in the middle of the transition, since coupling is directly related to the local slope, that is now larger. Total coupling is larger, as shown in Fig. 9(a) and (b) and radiation patterns of the linear transition and of the raised cosine one are reported in Fig. 10(a)–(d), for $s = 2\ \mu\text{m}$.

An asymmetrical transition was also been investigated, as shown in Fig. 5; in this case, only the fundamental (even) mode is excited in the incoming guide. Due to the asymmetry of the structure, coupling occurs between all modes of any parity. Consequently, as shown in Fig. 11, power is distributed over all modes, guided and continuous, even though only one mode is excited in the incoming guide. The radiation pattern is reported in Fig. 12, where $P_{\max} = 0.74$ W/(m · rad): asymmetry is evident and larger radiation occurs in the direction where the arm varies.

The effect of the length of the junction are reported in Fig. 13, for both polarizations; the curves refer to the case of excitation of the fundamental mode, with $t = 0.2\ \mu\text{m}$.

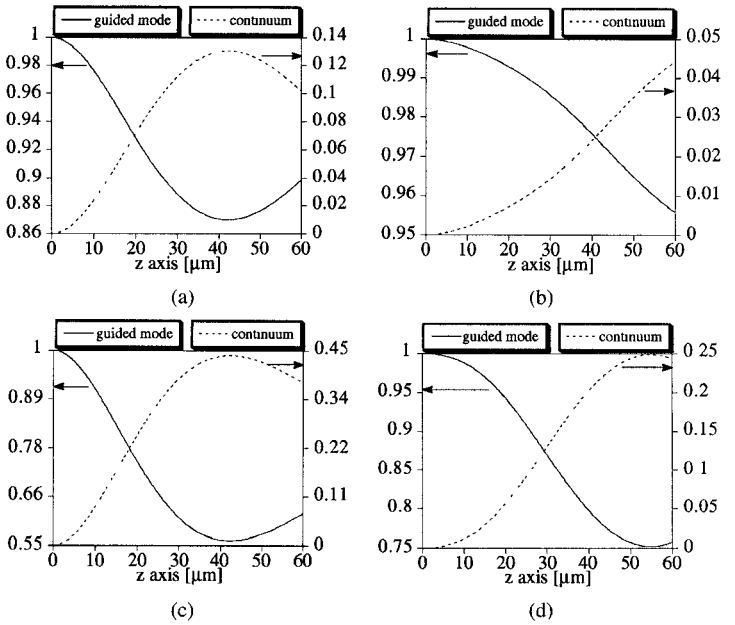

Fig. 8. The distribution of the normalized modal power along a linear transition, characterized by $n_1 = 3.44$, $n_2 = 3.40$, $t = 0.4$ μm, $d = 0.6$ μm, $\lambda = 1.15$ μm, $w_1 = w_2 = 1.5$ μm, $L = 60$ μm.The final separation is $s = 2$ μm in (a), (b), and $s = 4$ μm in (c), (d); (a) and (c) refer to the fundamental even mode and to the even continuum; (b) and (d) refer to the first higher odd mode and to the odd continuum.

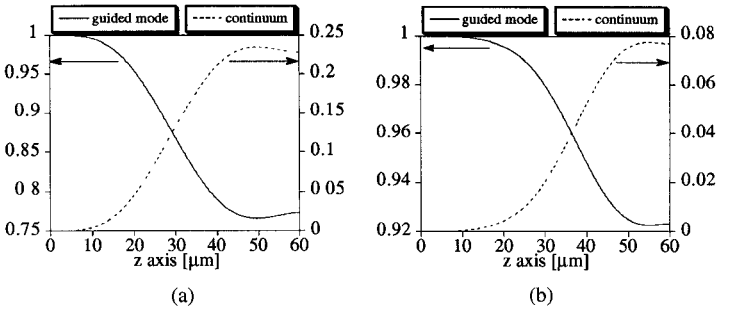

Fig. 9. The distribution of the normalized modal power along a raised cosine transition, characterized by the same parameters as in Fig. 8. The final separation is $s = 2$ μm. (a) refers to the fundamental even mode and to the even continuum; (b) refers to the first higher odd mode and to the odd continuum.

As we can expect, radiation is less excited by increasing the length of the junction, the coupling coefficients depending on the rapidity of the transition.

Finally, we analyzed the effect on modal coupling of changing the height, t, of the rib, with $L = 40$ μm: these effects are shown in Fig. 14, where the powers of the guided fundamental mode and of the continuum are reported for both cases of polarization. We note the presence of a maximum of radiation at about $t = 0.35$ μm: this is the combination of two effects. In fact, when the height t of the rib is very small, the y-junction disappears and, consequently, the loss is very small. On the other hand, when the height t of the rib is large, the field is well confined, feeling to a lesser extent the effects of the transition, so that, coupling coefficients and losses are lower; between these two areas of low loss, there is a maximum of loss, as reported in Fig. 14.

IV. Conclusion

We investigated the radiation of Y-junctions in dielectric rib waveguide by the method of local modes using the full continuous spectrum of an equivalent five-layer slab guide obtained by the EDC approach. Radiation patterns in the horizontal plane and loss are provided for symmetric and asymmetric Y-junctions, with linear and continuous tapering, under LSE and LSM polarizations.

Symmetry is seen to play a far greater role than the details of the tapering in determining the radiation characteristics of the junction.

Appendix A

In the hypothesis of LSE polarization, introducing (1) and (2) in (4) and taking into account (3), by some manipulations [12], we obtain

$$C_n'(z) + j\beta_n(z)C_n(z) = \sum_{k=-N}^{N} A_{nk}(z)C_k(z) + \sum_{\mu=\pm}\int_0^{\infty} A_{n\mu}(\rho,z) \cdot C_\mu(\rho,z)\,d\rho, \qquad n = -N\cdots N \tag{A1}$$

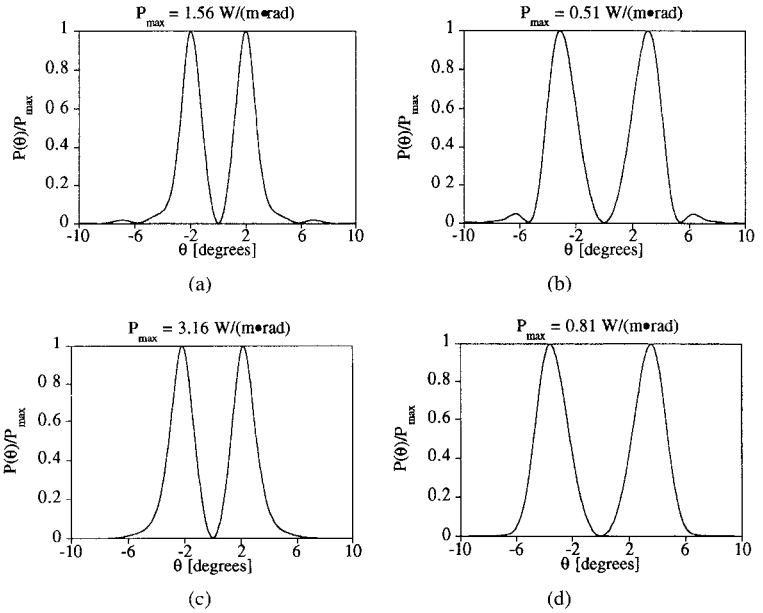

Fig. 10. Normalized radiation patterns for various transitions, with the same characteristics of Fig. 9: (a) radiation due to the even continuum of a linear transition; (b) radiation due to the odd continuum of a linear transition; (c) radiation due to the even continuum of a raised cosine transition; (d) radiation due to the odd continuum of a raised cosine transition.

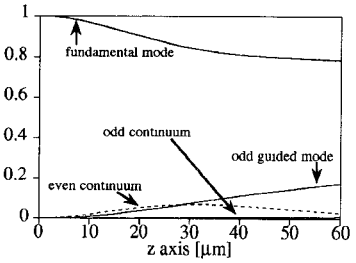

Fig. 11. Normalized modal power of a transition with one arm only varying along the z-direction, as shown in Fig. 5. The parameters are the same of Fig. 8. The final separation is $s = 2$ μm.

$$C'_\nu(\rho,z)+j\beta_\nu(\rho)C_\nu(\rho,z) = \sum_{k=-N}^{N} D_{\nu k}(\rho,z)C_k(z)+\sum_{\mu=\pm}\int_0^\infty D_{\nu\mu}(\rho,\tilde\rho,z)\cdot C_\mu(\tilde\rho,z)\,d\tilde\rho,\qquad \nu=\pm \tag{A2}$$

where the apex stands for derivation with respect to z and the coupling coefficients are given by

$$A_{nk}(z) = -\frac{\beta'_n(z)}{2\beta_n(z)}\delta_{nk}-\left\langle\frac{\Phi_n[x,(z)]\Phi'_k[x,(z)]}{2\varepsilon_e(x,z)}\right\rangle - \frac{\beta_k(z)}{2\beta_n(z)}\left\langle\Phi_n[x,(z)]\left[\frac{\Phi_k[x,(z)]}{\varepsilon_e(x,z)}\right]'\right\rangle$$

$$A_{n,n}(z) = -\frac{\beta'_n(z)}{2\beta_n(z)}$$

$$A_{n,-n}(z) = \frac{\beta'_n(z)}{2\beta_n(z)}$$

$$A_{n\mu}(\rho,z) = -\left\langle\frac{\Phi_n[x,(z)]\Phi'_\mu[\rho,x,(z)]}{2\varepsilon_e(x,z)}\right\rangle - \frac{\beta_\mu(\rho)}{2\beta_n(z)}\left\langle\Phi_n[x,(z)]\left[\frac{\Phi_\mu[\rho,x,(z)]}{\varepsilon_e(x,z)}\right]'\right\rangle$$

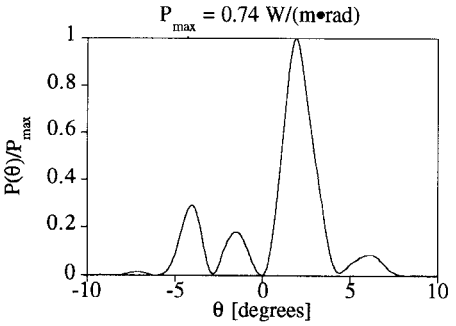

Fig. 12. The radiation pattern of the transition shown in Fig. 5. The continua of both parities contribute to radiation, producing an asymmetric pattern.

$$D_{\nu k}(\rho,z) = -\left\langle\frac{\Phi_\nu[\rho,x,(z)]\Phi'_k[x,(z)]}{2\varepsilon_e(x,z)}\right\rangle - \frac{\beta_k(z)}{2\beta_\nu(\rho)}\left\langle\Phi_\nu[\rho,x,(z)]\left[\frac{\Phi_k[x,(z)]}{\varepsilon_e(x,z)}\right]'\right\rangle$$

$$D_{\nu\mu}(\rho,\tilde\rho,z) = -\left\langle\frac{\Phi_\nu[\rho,x,(z)]\Phi'_\mu[\tilde\rho,x,(z)]}{2\varepsilon_e(x,z)}\right\rangle - \frac{\beta_\mu(\tilde\rho)}{2\beta_\nu(\rho)}\left\langle\Phi_\nu[\rho,x,(z)]\left[\frac{\Phi_\mu[\tilde\rho,x,(z)]}{\varepsilon_e(x,z)}\right]'\right\rangle.$$

Let us now express the coupling coefficients in simpler form. Multiplying (3) by $[\Phi_n[x,(z)]/k_0^2\varepsilon_e(x,z)]$ $(n\neq k)$, integrating over the cross-section, recalling the first Green's identity and differentiating w.r.t. z, we obtain

$$\langle\Phi_n[x,(z)]\Phi'_k[x,(z)]\rangle+\langle\Phi_k[x,(z)]\Phi'_n[x,(z)]\rangle = \left\langle\left[\frac{1}{k_0^2\varepsilon_e(x,z)}\right]'\frac{\partial\Phi_k[x,(z)]}{\partial x}\frac{\partial\Phi_n[x,(z)]}{\partial x}\right\rangle + \left\langle\frac{1}{k_0^2\varepsilon_e(x,z)}\frac{\partial}{\partial z}\left\{\frac{\partial\Phi_k[x,(z)]}{\partial x}\frac{\partial\Phi_n[x,(z)]}{\partial x}\right\}\right\rangle. \tag{A3}$$

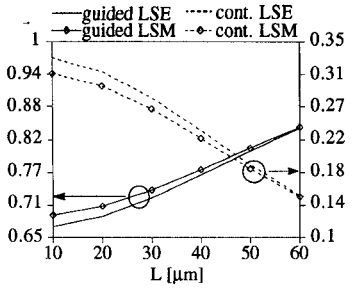

Fig. 13. Normalized modal power at the end of a linear transition versus its length L, for LSE and LSM polarizations. The parameters are the same of Fig. 8. Powers of the guided modes are shown as continuous lines.

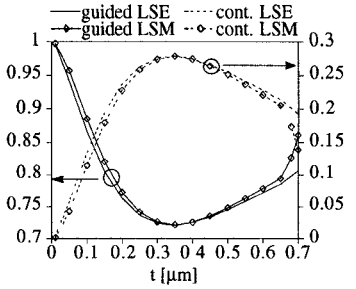

Fig. 14. Normalized modal power at the end of a linear transition versus height, t, of the rib, for LSE and LSM polarizations. The parameters are the same of Fig. 8, with $L = 40$ μm. Powers of the guided modes are shown as continuous lines.

Multiplying (3) by $\Phi_k'[x,(z)]/k_0^2\varepsilon_e(x,z)$, we obtain analogously

$$\langle \Phi_n[x,(z)]\Phi_k'[x,(z)]\rangle - \beta_n^2(z)\left\langle \frac{\Phi_n[x,(z)]\Phi_k'[x,(z)]}{k_0^2\varepsilon_e(x,z)}\right\rangle = \left\langle \frac{1}{k_0^2\varepsilon_e(x,z)}\frac{\partial\Phi_k'[x,(z)]}{\partial x}\frac{\partial\Phi_n[x,(z)]}{\partial x}\right\rangle. \quad \text{(A4a)}$$

Similarly

$$\langle \Phi_k[x,(z)]\Phi_n'[x,(z)]\rangle - \beta_k^2(z)\left\langle \frac{\Phi_k[x,(z)]\Phi_n'[x,(z)]}{k_0^2\varepsilon_e(x,z)}\right\rangle = \left\langle \frac{1}{k_0^2\varepsilon_e(x,z)}\frac{\partial\Phi_n'[x,(z)]}{\partial x}\frac{\partial\Phi_k[x,(z)]}{\partial x}\right\rangle. \quad \text{(A4b)}$$

Summing (A4a) and (A4b), changing sign and substituting in (A3) yields

$$[\beta_n^2(z)-\beta_k^2(z)]\left\langle \frac{\Phi_n[x,(z)]\Phi_k'[x,(z)]}{\varepsilon_e(x,z)}\right\rangle = \left\langle \left[\frac{1}{\varepsilon_e(x,z)}\right]'\frac{\partial\Phi_n[x,(z)]}{\partial x}\frac{\partial\Phi_k[x,(z)]}{\partial x}\right\rangle + \beta_k^2(z)\left\langle \left[\frac{1}{\varepsilon_e(x,z)}\right]'\Phi_n[x,(z)]\Phi_k[x,(z)]\right\rangle. \quad \text{(A5)}$$

Substituting (A5) in the expression of $A_{nk}(n\neq k)$ yields

$$A_{nk} = -\frac{1}{2\beta_n(z)[\beta_n(z)-\beta_k(z)]}\cdot\left\{\beta_n(z)\beta_k(z)\left\langle\left[\frac{1}{\varepsilon_e(x,z)}\right]'\Phi_n[x,(z)]\Phi_k[x,(z)]\right\rangle - \left\langle\frac{\varepsilon_e'(x,z)}{\varepsilon_e^2(x,z)}\frac{\partial\Phi_n[x,(z)]}{\partial x}\frac{\partial\Phi_k[x,(z)]}{\partial x}\right\rangle\right\}. \quad \text{(A6)}$$

Since $\Phi_n[x,(z)]$ and $[1/\varepsilon_e(x,z)][\partial\Phi_n[x,(z)]/\partial x]$ are continuous functions across the interfaces $f_i(z)$, denoting by $f_i^+(z)$ and $f_i^-(z)$ the profiles evaluated at $x=x_i^+$ and $x=x_i^-$ on the z-plane and recalling that

$$\left[\frac{1}{\varepsilon_e(x,z)}\right]' = \sum_{i=1}^{4} f_i'(z)\left\{\frac{\delta[x-f_i^+(z)]}{\varepsilon_e[f_i^+(z),z]}-\frac{\delta[x-f_i^-(z)]}{\varepsilon_e[f_i^-(z),z]}\right\}$$

$$\varepsilon_e'(x,z) = -\sum_{i=1}^{4} f_i'(z)\{\delta[x-f_i^+(z)]\varepsilon_e[f_i^+(z),z] - \delta[x-f_i^-(z)]\varepsilon_e[f_i^-(z),z]\}$$

(A6), for $n\neq k$, becomes

$$A_{nk} = \frac{1}{2\beta_n(z)[\beta_n(z)-\beta_k(z)]}\sum_{i=1}^{4} T_{ink}(z) \quad \text{(A7)}$$

with

$$T_{1nk} = f_1'(z)\frac{\varepsilon_{e1}-\varepsilon_{e2}}{\varepsilon_{e1}\varepsilon_{e2}}\left\{U_{nk}+\frac{\varepsilon_{e1}}{\varepsilon_{e2}}V_{nk}\right\}_{x=f_1^+(z)}$$

$$T_{2nk} = f_2'(z)\frac{\varepsilon_{e2}-\varepsilon_{e1}}{\varepsilon_{e1}\varepsilon_{e2}}\left\{U_{nk}+\frac{\varepsilon_{e2}}{\varepsilon_{e1}}V_{nk}\right\}_{x=f_2^+(z)}$$

$$T_{3nk} = f_3'(z)\frac{\varepsilon_{e1}-\varepsilon_{e2}}{\varepsilon_{e1}\varepsilon_{e2}}\left\{U_{nk}+\frac{\varepsilon_{e2}}{\varepsilon_{e1}}V_{nk}\right\}_{x=f_3^-(z)}$$

$$T_{4nk} = f_4'(z)\frac{\varepsilon_{e2}-\varepsilon_{e1}}{\varepsilon_{e1}\varepsilon_{e2}}\left\{U_{nk}+\frac{\varepsilon_{e1}}{\varepsilon_{e2}}V_{nk}\right\}_{x=f_4^-(z)}$$

$$U_{nk} = \beta_n(z)\beta_k(z)\Phi_n[x,(z)]\Phi_k[x,(z)]$$

$$V_{nk} = \frac{\partial\Phi_n[x,(z)]}{\partial x}\frac{\partial\Phi_k[x,(z)]}{\partial x}$$

Analogous expressions hold for the other coupling coefficients.

In the case of LSM polarization, the expression of the coupling coefficient A_{nk} is

$$A_{nk} = -\frac{k_0^2}{2\beta_n(z)[\beta_n(z)-\beta_k(z)]}\sum_{i=1}^{4} T_{ink}(z) \quad \text{(A8)}$$

with

$$T_{1nk} = f_1'(z)(\varepsilon_{e2}-\varepsilon_{e1})\{\Phi_n[x,(z)]\Phi_k[x,(z)]\}_{x=f_1^+(z)}$$

$$T_{2nk} = f_2'(z)(\varepsilon_{e1}-\varepsilon_{e2})\{\Phi_n[x,(z)]\Phi_k[x,(z)]\}_{x=f_2^+(z)}$$

$$T_{3nk} = f_3'(z)(\varepsilon_{e2}-\varepsilon_{e1})\{\Phi_n[x,(z)]\Phi_k[x,(z)]\}_{x=f_3^-(z)}$$

$$T_{4nk} = f_4'(z)(\varepsilon_{e1}-\varepsilon_{e2})\{\Phi_n[x,(z)]\Phi_k[x,(z)]\}_{x=f_4^-(z)}.$$

APPENDIX B

To solve (7a) and (8a), we set

$$H_n(z) = a_{ni} + b_{ni}[z-(i-1)\Delta z] + c_{ni}[z-(i-1)\Delta z]^2 \tag{B1}$$

$$H_n'(z) = b_{ni} + 2c_{ni}[z-(i-1)\Delta z] \qquad (i-1)\Delta z \le z \le i\Delta z, \qquad i = 1\cdots M \tag{B2}$$

where $M\Delta z = L$. In (B1) and (B2), the coefficients a_{ni} and b_{ni} are obtained by imposing the continuity of $H_n(z)$ and $H_n'(z)$ at $z = (i-1)\Delta z$, thus ensuring satisfaction of the boundary conditions. We suppose that in each subinterval $(i-1)\Delta z \le z \le i\Delta z$ the following quantities are locally constant

$$\begin{aligned}
A_{nk} &\approx A_{nk}(i\Delta z), \quad A_{n\mu}(\rho, z) \approx A_{n\mu}(\rho, i\Delta z)\\
D_{\mu k} &\approx D_{\mu k}(\rho, i\Delta z), \quad \beta_n(z) \approx \beta_n(i\Delta z)\\
\gamma_n &\approx (z - i\Delta z)\tan\alpha_{ni} + \gamma_n(i\Delta z)\\
\tan\alpha_{ni} &= \frac{\gamma_n(i\Delta z) - \gamma_n[(i-1)\Delta z]}{\Delta z}\\
\theta_{ni}(\rho) &= [\tan\alpha_{ni} - \beta(\rho)]\Delta z\\
P_{nki} &= \sqrt{\frac{\beta_n(i\Delta z)}{\beta_k(i\Delta z)}}\, e^{j[\gamma_n(i\Delta z) - \gamma_k(i\Delta z)]}
\end{aligned}$$

Integration of (8a) w.r.t. z in the range $(i-1)\Delta z \le z \le i\Delta z$ yields

$$\begin{aligned}
H_\mu(\rho, i\Delta z) = H_\mu[\rho, (i-1)\Delta z] + \sum_{k=1}^{N} D_{\mu k}(\rho, i\Delta z)\beta(\rho)\\
\cdot \frac{e^{-j[\gamma_k(i\Delta z) - \beta(\rho)i\Delta z]}}{\sqrt{\beta_k(i\Delta z)}} \left\{ j\frac{a_{k,i+1} - a_{ki}e^{j\theta_{ki}(\rho)}}{\theta_{ki}(\rho)} \right.\\
\cdot \Delta z + \frac{b_{ki}[1 - e^{j\theta_{ki}(\rho)}] + 2c_{ki}\Delta z}{\theta_{ki}^2(\rho)}\\
\left. \cdot \Delta z^2 - 2jc_{ki}\frac{1 - e^{j\theta_{ki}(\rho)}}{\theta_{ki}^3(\rho)}\Delta z^3 \right\}.
\end{aligned} \tag{B3}$$

Moreover, (7a) at $z = i\Delta z$ yields

$$\begin{aligned}
H_n'(i\Delta z) = b_{ni} + 2c_{ni}\Delta z = \sum_{\substack{k=1\\k\neq n}}^{N} P_{nki}A_{nk}(i\Delta z)H_k(i\Delta z)\\
+ \sum_{\mu=e,o}\int_0^\infty A_{n\mu}(\rho, i\Delta z)H_\mu(\rho.i\Delta z)\frac{\sqrt{\beta_n(i\Delta z)}}{\beta(\rho)}\\
\cdot e^{j[\gamma_n(i\Delta z) - \beta(\rho)i\Delta z]}\, d\rho.
\end{aligned} \tag{B4}$$

Substituting (B1), (B2), and (B3) in (B4), after some manipulations, yields a system of linear equations for the unknowns c_{ni}

$$\begin{aligned}
c_{ni}(2\Delta z - J_{nni}\Delta z^2 - 2L_{nni})\\
= \sum_{\substack{k=1\\k\neq n}}^{N} P_{nki}c_{ki}[A_{nk}(i\Delta z)\Delta z^2 + J_{nki}\Delta z^2 + 2L_{nki}]\\
+ S_{ni} + \sum_{k=1}^{N} P_{nki}[A_{nk}(i\Delta z)(a_{ki} + b_{ki}\Delta z) + a_{ki}I_{nki}\\
+ b_{ki}(K_{nki} + J_{nki}\Delta z)] - b_{ni}, \qquad n = 1\cdots N
\end{aligned} \tag{B5}$$

where

$$\begin{aligned}
S_{ni} &= \sum_{\mu=e,o}\int_0^\infty \frac{\sqrt{\beta_n(i\Delta z)}}{\beta(\rho)}A_{n\mu}(\rho, i\Delta z)\\
&\quad \cdot H_\mu[\rho, (i-1)\Delta z]e^{j[\gamma_n(i\Delta z) - \beta(\rho)i\Delta z]}\, d\rho\\
I_{nki} &= j\Delta z\sum_{\mu=e,o}\int_0^\infty A_{n\mu}(\rho, i\Delta z)D_{\mu k}(\rho, i\Delta z)\\
&\quad \cdot \frac{1 - e^{j\theta_{ki}(\rho)}}{\theta_{ki}(\rho)}d\rho\\
J_{nki} &= j\Delta z\sum_{\mu=e,o}\int_0^\infty \frac{A_{n\mu}(\rho, i\Delta z)D_{\mu k}(\rho, i\Delta z)}{\theta_{ki}(\rho)}d\rho\\
K_{nki} &= \Delta z^2\sum_{\mu=e,o}\int_0^\infty A_{n\mu}(\rho, i\Delta z)D_{\mu k}(\rho, i\Delta z)\\
&\quad \cdot \frac{1 - e^{j\theta_{ki}(\rho)}}{\theta_{ki}^2(\rho)}d\rho\\
L_{nki} &= \Delta z^3\sum_{\mu=e,o}\int_0^\infty A_{n\mu}(\rho, i\Delta z)D_{\mu k}(\rho, i\Delta z)\\
&\quad \cdot \frac{\theta_{ki}(\rho) - j[1 - e^{j\theta_{ki}(\rho)}]}{\theta_{ki}^3(\rho)}d\rho.
\end{aligned}$$

Once (B5) is obtained, our problem is solved. In fact, in the hypothesis that continuous modes are not incident at the beginning of the transition ($z = 0$), we obtain the amplitude of the coefficients a_{n1} and b_{n1} from the incident power

$$\begin{aligned}
a_{n1} &= \sqrt{2\omega\varepsilon_0 P_n}\\
b_{n1} &= H_n'(0) = \sum_{\substack{k=1\\k\neq n}}^{N} A_{nk}(0)a_{k1}\sqrt{\frac{\beta_n(0)}{\beta_k(0)}},\\
&\qquad n = 1\cdots N
\end{aligned} \tag{B6}$$

Then, solution of (B5) yields the value of c_{n1} and (B3) yields the expression of $H_\mu(\rho, \Delta z)$ being $H_\mu(\rho, 0) = 0$. For the ith section, the procedure is very simple:

1) from the conditions at $z = (i-1)\Delta z$ we obtain a_{ni}, b_{ni} and from (B3) $H_\mu[\rho, (i-1)\Delta z]$;
2) from (B5) we obtain c_{ni}, from (B1) and (B2) $a_{n,i+1} = a_{ni} + b_{ni}\Delta z + c_{ni}\Delta z^2, b_{n,i+1} = b_{ni} + 2c_{ni}\Delta z$ and, finally, from (B3) $H_\mu(\rho, i\Delta z)$;
3) with these new values we resume at point 1).

REFERENCES

[1] T. Tamir, "Guided-wave optoelectronics," 2nd Ed. New York: Springer-Verlag, 1990.

[2] H. Yajima, "Coupled mode analysis of dielectric planar branching waveguides," *IEEE J. Quant. Electron.*, vol. QE-14, no. 10, pp. 749–755, Oct. 1978.

[3] W. K. Burns and A. F. Milton, "An analytical solution for mode coupling in optical waveguide branches," *IEEE J. Quant. Electron.*, vol. QE-16, no. 4, pp. 446–454, Apr. 1980.

[4] M. Tsuji, O. Tanaka, and H. Shigesawa, "Low-loss design method for a planar dielectric-waveguide Y branch: Effect of a taper of serpentine shape," *IEEE Trans. Microwave Theory Tech.*, vol. MTT-39, no. 1, pp. 6–13, Jan. 1991.
[5] W.-P. Huang and B. E. Little, "Power exchange in tapered optical couplers," *IEEE J. Quant. Electron.*, vol. 27, no. 7, pp. 1932–1938, July 1991.
[6] G. H. Song and W. J. Tomlinson, "Fourier analysis and synthesis of adiabatic tapers in integrated optics," *J. Opt. Soc. Am. A*, vol. 9, no. 8, pp. 1289–1300, Aug. 1992.
[7] D. Yevick and B. Hermansson, "Split-step finite difference analysis of rib waveguides," *Electron. Lett.*, vol. 25, no. 7, pp. 461–462, Mar. 1989.
[8] D. Yevick and M. Glasner, "Analysis of forward wide-angle light propagation in semiconductor rib waveguides and integrated-optic structures," *Electron. Lett.*, vol. 25, no. 23, pp. 1611–1613, Nov. 1989.
[9] D. Yevick and B. Hermansson, "Efficient beam propagation techniques," *IEEE J. Quant. Electron.*, vol. 26, no. 1, pp. 109–112, Jan. 1990.
[10] V. V. Shevchenko, *Continuous Transition in Open Waveguides*. Boulder, CO: Golem Press, 1971.
[11] T. Rozzi, G. Cerri, F. Chiaraluce, R. De Leo, and R. Ormondroyd, "Finite curvature and corrugations in dielectric ridge waveguides," *IEEE Trans. Microwave Theory Tech.*, vol. 36, no. 1, pp. 68–79, Jan. 1988.
[12] T. Rozzi, L. Zappelli, and M. N. Husain, "Radiation modes and step discontinuities in dielectric rib waveguide," *IEEE Trans. Microwave Theory Tech.*, vol. 40, no. 10, pp. 1879–1888, Oct. 1992.
[13] T. Rozzi, F. Chiaraluce, and M. Lanari, "A rigourous analysis of DFB lasers with large and aperiodic corrugations," *IEEE J. Quant. Electron.*, vol. 27, no. 2, pp. 212–223, Feb. 1991.
[14] D. Marcuse, *Light Transmission Optics*, 2nd Ed. New York: Van Nostrand, 1982.

Lucia Cascio (S'95) was born in Fano, Italy, in 1967. She received the degree (summa cum laude) in electronic enginnering from the University of Ancona, Ancona, Italy, in 1993. In 1993 she was awarded a scholarship by the Italian National Research Council for a full time research program in the field of electro-optical technologies.

Currently, she is a Research Assistant working toward her Ph.D. in electronic engineering at the University of Victoria, Victoria B.C., Canada. Her current research is in the area of analytical and numerical modeling of microwave circuits.

Tullio Rozzi (M'66–SM'74–F'90) received the degree of dottore in physics from the University of Pisa in 1965, and the Ph.D. degree in electronic engineering from the Leeds University in 1968. In 1987 he received the D.Sc. degree from the University of Bath, Bath, U.K.

From 1968–1978 he was a Research Scientist at the Philips Research Laboratories, Eindhoven, The Netherlands, having spent one year at the Antenna Laboratory, University of Illinois, Urbana. In 1978 he was appointed to the Chair of Electrical Engineering at the University of Liverpool and was subsequently appointed to the Chair of Electronics and Head of the Electronics Group at the University of Bath, in 1981, where he also held the responsibility of Head of the School of Electrical Engineering on an alternate three-year basis. Since 1988 he has been Professor of Antennas in the Department of Electronics and Automatics, University of Ancona, Italy, while remaining a Visiting Professor at Bath University.

Dr. Rozzi was awarded the Microwave Prize by the IEEE Microwave Theory and Technique Society in 1975. He is also a Fellow of the IEE (U.K.)

Leonardo Zappelli was born in Rome in 1962. He received the doctor degree in electronic engineering from the University of Ancona, Italy, in 1987 and the Ph.D. degree in electromagnetics from the University of Ancona, Italy, in 1992.

Since 1988, he has been with the Department of Electronics and Automatics, University of Ancona, Italy. His current research interests are integrated optics, microwaves, and electromagnetic compatibility.